

## Laboratory testing the Anaconda

BY J. R. CHAPLIN<sup>1,\*</sup>, V. HELLER<sup>1,†</sup>, F. J. M. FARLEY<sup>1</sup>, G. E. HEARN<sup>2</sup>  
AND R. C. T. RAINEY<sup>1,3</sup>

<sup>1</sup>*School of Civil Engineering and the Environment, and* <sup>2</sup>*School of Engineering Sciences, University of Southampton, Southampton SO17 1BJ, UK*

<sup>3</sup>*Oil and Gas Division, Atkins, Ashley Road, Epsom KT18 5BW, UK*

Laboratory measurements of the performance of the Anaconda are presented, a wave energy converter comprising a submerged water-filled distensible tube aligned with the incident waves. Experiments were carried out at a scale of around 1 : 25 with a 250 mm diameter and 7 m long tube, constructed of rubber and fabric, terminating in a linear power take-off of adjustable impedance. The paper presents some basic theory that leads to predictions of distensibility and bulge wave speed in a pressurized compound rubber and fabric tube, including the effects of inelastic sectors in the circumference, longitudinal tension and the surrounding fluid. Results are shown to agree closely with measurements in still water. The theory is developed further to provide a model for the propagation of bulges and power conversion in the Anaconda. In the presence of external water waves, the theory identifies three distinct internal wave components and provides theoretical estimates of power capture. For the first time, these and other predictions of the behaviour of the Anaconda, a device unlike almost all other marine systems, are shown to be in remarkably close agreement with measurements.

**Keywords:** wave power; wave energy converter; linear power take-off;  
pressure wave propagation

### 1. Introduction

The basic principles of the Anaconda wave energy converter have been explained by Farley *et al.* [1]. The device consists of a pressurized water-filled distensible tube aligned with the water waves and floating just beneath the surface. Wave-induced external pressures generate travelling bulges and contractions in the tube that grow with distance, and deliver an oscillating internal flow, several times stronger than that in the undisturbed water waves, to a power take-off (PTO) at the down-wave end (or stern).

Among offshore systems, the Anaconda has some features in common with dracones, which are long flexible tubes designed to be towed across the sea, carrying oil or other light liquids. Dracones are buoyant and are only partially

\*Author for correspondence ([j.r.chaplin@soton.ac.uk](mailto:j.r.chaplin@soton.ac.uk)).

†Present address: Department of Civil and Environmental Engineering, Imperial College, London SW7 2AZ, UK.

One contribution of 18 to a Theo Murphy Meeting Issue ‘The peaks and troughs of wave energy: the dreams and the reality’.

filled, retaining some air above the internal liquid. Some full-scale tests and theoretical studies were carried out in the 1950s, and were reported by Hawthorne [2]. Besides addressing the issues of materials and construction, this research concentrated on the analysis of the static shape of a floating flexible tube that is partially filled, and of the stability of the tube under tow. Besides the problem of snaking in forward motion, the tube was vulnerable to large pressures developed by longitudinal surging of the internal liquid. This was not primarily associated with the bulge waves that are of interest here, because the dracones were constructed from nylon material which was practically inextensible. Thus, the surges were accompanied not by bulges and contractions in the tube, but by violent longitudinal motion of the air in the upper part of its cross section. Hawthorne set out a theory for the snaking, but did not present any analysis of internal surges. A linear numerical solution of the problem of motion of a dracone towed in head waves is described by Zhao & Triantafyllou [3]; the theory included longitudinal bending of the tube, but its skin was assumed to be inelastic in the transverse direction, in accordance with the construction of the actual dracones. The design of the dracone experiments [4] had to overcome some problems similar to those faced in the present case, and tests on the Anaconda made use of the same basic technique for measuring large strains in rubber, described in detail in §3.

Wave propagation in fluid-filled distensible tubes (as opposed to partially filled inelastic tubes) has long been the subject of research (for reviews see [5–7]), much of it in connection with modelling the cardiovascular system. Since blood viscosity is clearly a factor, a frequent starting point for modelling the flow in blood vessels (e.g. [8–10]) is Womersley’s solution [11] for the oscillatory motion of a viscous fluid in a thin-walled elastic tube. In fact, many studies use simplified approximations of Womersley’s velocity profiles, such as a Stokes layer near the boundaries with a central uniform core, a power law, the Poiseuille profile or even simply uniform flow [5]. The last of these is likely to provide a reasonable approximation for the high Reynolds number flow in the Anaconda, and some research in haemodynamics has focused on wave propagation in elastic tubes in a related way, treating the liquid as incompressible and inviscid [12–14].

For present purposes, a key property of an elastic-walled tube is its distensibility  $D$ , defined by

$$D = \frac{1}{S} \frac{dS}{dp}, \quad (1.1)$$

where  $S$  is its internal area and  $p$  the pressure difference across the tube wall (assuming that any changes take place slowly). In the ‘linear long wavelength’ (LLW) theory, which can be traced back to Young [15], the wavelength is assumed to be much greater than the diameter, and the material of the tube wall is assumed to be loss-free. Convective accelerations are neglected. Wave propagation is controlled solely by distensibility and the longitudinal inertia of the contained liquid. In the LLW theory, waves are non-dispersive and undamped and travel at a speed  $c$  given by [16]

$$c = (\rho D)^{-1/2}, \quad (1.2)$$

where  $\rho$  is the fluid density. (In the biology literature, equation (1.2) is known as the Moens–Korteweg formula.) When the conditions of the LLW theory are not met, bulges undergo a change in shape, becoming broader and weaker as

they advance (e.g. [17,18]). Investigating this process analytically for inviscid incompressible fluid in a thin-walled tube, Moodie *et al.* [13] concluded that the next most important effects, in order after distensibility and fluid inertia, would be losses in the tube wall, radial inertia of fluid and wall, and bending stiffness and rotary inertia of the wall. Just the first of these accounted for a large part of the observed transformation. In the case of the Anaconda, other factors enter the problem, namely inextensible sectors in the tube's circumference, longitudinal tension in the tube walls and the inertia of water surrounding the tube.

The aim of the work described in this paper was to improve our understanding of the generation and propagation of bulge waves in the Anaconda at model scale, and to compare measured power capture with the predictions of a simple one-dimensional theory. It was not our aim to optimize the performance of the device or to attempt to show that it may be capable of operating on an industrial scale. The one-dimensional theory, described in §2, extends the LLW theory to the case of a tube of finite length and non-zero hysteresis, closed at one end and with a PTO at the other. It neglects the effects of surface wave diffraction and radiation. Section 3 outlines arrangements for the experiments, the results of which are presented and discussed in §§4 and 5. Many features of the measurements are found to be in remarkable agreement with predictions.

## 2. Theoretical background

This section outlines some theory on various aspects of the problem, with the aim of providing a useful background for discussion of the measurements.

### (a) *Distensibility of a tube with inextensible circumferential sectors, axially restrained*

Let  $R_0$  be the radius of the unstressed tube and  $h_0$  the corresponding wall thickness. In the experiments, the tube was made of rubber but, in order to postpone the onset of aneurysm (see [1]), part of its circumference was covered in longitudinal fabric strips glued to the external surface. The fabric was virtually inextensible. Therefore, when the tube was pressurized, all of the circumferential expansion took place in the sectors of uncovered rubber, accounting for a proportion initially  $\alpha$  of the total circumference.

Suppose that, when the internal pressure exceeds the external pressure by  $p$ , the tube has a radius of say  $R$  and a wall thickness of say  $h$ . The hoop strain in the rubber is then  $\varepsilon_h = (R - R_0)/\alpha R_0$ . The pressure difference across the wall is balanced by the product of the hoop tension per unit length in the uncovered rubber  $\sigma_h h$ , where  $\sigma_h$  is the true hoop stress and the curvature of the wall  $1/R$ , thus  $\sigma_h = pR/h$ . If the ends of the tube are held in place (as in the experiment) and it does not move longitudinally (or, in the language of the biological literature, is tethered), then the rubber is in a state of plane strain, and  $\sigma_h = E\varepsilon_h/(1 - \nu^2)$ . (The stress in the rubber in the radial direction is much smaller than  $\sigma_h$ .) This, together with the assumptions [19] that rubber, being incompressible, has a Poisson's ratio  $\nu = 1/2$ , and that  $E$  is true stress divided by strain, leads to

$$p = \frac{4Eh_0}{3R_0} \frac{r' - 1}{r'(r' - 1 + \alpha)}, \quad (2.1)$$

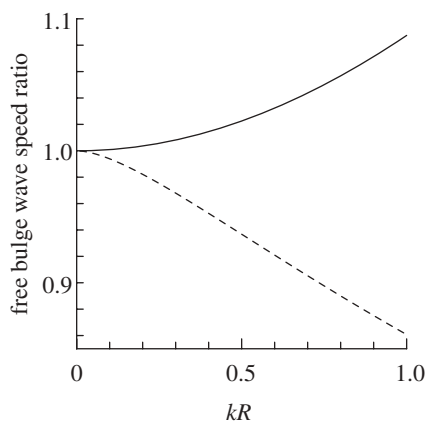


Figure 1. Relative changes in free bulge wave speed owing to the reduction in distensibility caused by longitudinal curvature in bulges (solid line), and owing to the presence of surrounding water (dashed line)  $\alpha = 0.45$ .

where  $r' = R/R_0$ . The corresponding distensibility is

$$D = \frac{3R_0}{2Eh_0} \frac{r'(r' - 1 + \alpha)^2}{\alpha - (r' - 1)^2}. \quad (2.2)$$

The pressure at which an aneurysm would appear (when  $dp/dR = 0$ ) is

$$p_{\text{crit}} = \frac{4Eh_0}{3R_0} \frac{1}{(1 + \alpha^{1/2})^2}, \quad (2.3)$$

at a radius of  $R_0(1 + \alpha^{1/2})$ . If the pressure  $p$  were zero, and the tube were constructed entirely of rubber ( $\alpha = 1$ ), the distensibility would be  $3R_0/2Eh_0$ . This is 25 per cent less than the result obtained by Lighthill [16] because here it is assumed that the tube is constrained longitudinally.

When bulges travel along a tube in axial tension, there is a reduction in distensibility caused by longitudinal curvature. Suppose the radius of the pressurized tube is  $R = R_1 + a \cos kx$ , where  $x$  is measured along its length, and  $R_1 > R_0$ . There is then an additional radial force per unit area in the tube, balancing an increment in the pressure drop across the wall. This is equal to the product of the longitudinal tension per unit circumferential length  $\sigma_x h$  (where  $\sigma_x$  is the longitudinal stress) and the longitudinal curvature  $k^2 a$ . Proceeding as before, with  $\sigma_x = \nu \sigma_h = \sigma_h/2$  (as in plane strain), the modified distensibility  $D'$  is given by

$$\frac{1}{D'} = \frac{1}{D} + \frac{1}{4} k^2 R_1^2 p. \quad (2.4)$$

The resulting relative increase in free bulge wave speed  $(D/D')^{1/2}$  is plotted as a function of  $kR$  in figure 1 for  $\alpha = 0.45$  for a tube having an internal pressure of 75 per cent of  $p_{\text{crit}}$  ( $R_1/R_0 = 1.219$ ).

For the experimental conditions described below (a tube of about 7 m long and 0.25 m in diameter), the increase in free bulge wave speed would be about 3.3 per cent, 0.21 per cent and 0.05 per cent for bulge wavelengths of 1 m,

4 m and 8 m, respectively. Since typical wavelengths in the experiments were towards the upper end of this range, the effect is neglected for present purposes, though it might be significant for short bulge waves with high longitudinal wall tension.

(b) *The influence of the surrounding water on free bulge wave speed*

Bulging motion in a submerged tube generates time-varying external pressures owing to the inertia of the surrounding water. These modify the effective distensibility and free bulge wave speed.

Consider an infinitely long deeply submerged tube of radius  $R$  conveying regular small amplitude bulge waves of angular frequency  $\omega$  and wavenumber  $k$ . The external flow generated by the passing bulges is equivalent to the effect of a continuous travelling source distributed along the centreline of the tube, which is taken to be the  $x$ -axis. If the source strength per unit length at  $x'$  is the real part of  $Ae^{i(kx' - \omega t)}$ , then the total potential at an arbitrary point in cylindrical polar coordinates  $(x, r)$  is the real part of

$$\phi = A \int_{-\infty}^{\infty} \frac{e^{i(kx' - \omega t)}}{\sqrt{(x - x')^2 + r^2}} dx' = 2AK_0(kr)e^{i(kx - \omega t)}, \quad (2.5)$$

where  $K_n$  is the modified Bessel function of the second kind of order  $n$ .

In developing the theory, it is helpful to extract the time-dependence, so a physical quantity  $p(x, t)$  is to be understood as being represented by the real part of  $P(x)e^{-i\omega t}$ , where  $P(x)$  is a complex amplitude.

On the mean surface of the tube  $r = R$ , the external pressure is  $P_e(x)e^{-i\omega t} = -\rho(\partial\phi/\partial t)_{r=R}$ . The internal pressure exceeds this by the bulge pressure  $P_b(x)e^{-i\omega t}$ , which is related to the tube's area  $S$  by the distensibility,

$$DS \frac{\partial}{\partial t} P_b(x)e^{-i\omega t} = \frac{\partial S}{\partial t} \quad \text{or} \quad -i\omega DSP_b(x) = 2\pi R \left. \frac{\partial\phi}{\partial r} \right|_{r=R}. \quad (2.6)$$

Substituting both pressures into the bulge wave equation for zero hysteresis [1],

$$-\omega^2 P_b = \frac{1}{\rho D} \frac{\partial}{\partial x^2} (P_e + P_b), \quad (2.7)$$

leads to the following result for the free bulge wave speed:

$$\frac{\omega}{k} = \frac{1}{\sqrt{\rho D}} \sqrt{\frac{2K_1(kR)}{2K_1(kR) + kRK_0(kR)}}. \quad (2.8)$$

The reduction in bulge wave speed caused by the presence of surrounding water is plotted in figure 1. For present purposes, this is also a small effect.

(c) *Bulge wave propagation with a basic power take-off and no hysteresis*

It is useful to formulate a one-dimensional model for the propagation of bulge waves in the Anaconda. The fundamentals are set out in Farley *et al.* [1], but here the boundary conditions are slightly different. It is assumed that the tube is submerged at a fixed elevation beneath regular water waves of angular frequency  $\omega$  and wavenumber  $k_w$ . The tube is closed and stationary at the

up-wave end (or bow),  $x=0$ , and there is a linear dashpot PTO at the stern,  $x=L$ . In this one-dimensional theory, diffraction and radiation of water waves are omitted.

The tube experiences an external pressure whose complex amplitude is  $P_e(x) = \rho g A e^{ik_w x}$ . The bulge pressure and the internal particle velocity (assumed uniform over the cross section) are similarly represented by their complex amplitudes  $P_b(x)$  and

$$U(x) = -\frac{i}{\rho\omega} \frac{d}{dx} (P_e + P_b). \quad (2.9)$$

A solution of the wave equation (2.7) is required, with boundary conditions  $U=0$  at  $x=0$  and  $U=(P_e + P_b)/\rho c$  at  $x=L$ . The latter represents a PTO that matches the tube's impedance,  $\rho c/S$ .

The solution is

$$\frac{P_b}{\rho g A} = \frac{k_w^2}{k_b^2 - k_w^2} e^{ik_w x} - \left[ \frac{k_w k_b}{k_b^2 - k_w^2} + \frac{k_b e^{i(k_b+k_w)L}}{2(k_b + k_w)} \right] e^{ik_b x} - \frac{k_b e^{i(k_b+k_w)L}}{2(k_b + k_w)} e^{-ik_b x}, \quad (2.10)$$

where  $k_b = \omega/c$  is the wavenumber of free bulge waves. The first three terms on the right-hand side represent waves travelling in the positive  $x$  direction, the first (hereafter denoted  $p_w^+$ ) with the water wave speed  $\omega/k_w$ , and the second and third together ( $p_b^+$ ) with the free bulge wave speed  $c$ . The fourth term ( $p_b^-$ ) is also a wave with speed  $c$ , but travelling in the opposite direction.

The third and fourth terms represent a standing wave, so an alternative formulation of equation (2.10) is

$$\frac{P_b}{\rho g A} = \frac{k_w}{k_b^2 - k_w^2} [k_w e^{ik_w x} - k_b e^{ik_b x}] - \frac{k_b e^{i(k_b+k_w)L}}{k_b + k_w} \cos k_b x. \quad (2.11)$$

At  $x=0$ ,

$$\frac{P_e + P_b}{\rho g A} = \frac{k_b}{k_b + k_w} [1 - e^{i(k_b+k_w)L}], \quad (2.12)$$

indicating that the total internal pressure is zero at the bow when

$$(k_w + k_b)L = 2n\pi \quad (2.13)$$

and  $n$  is an integer.

At resonance,  $k_b = k_w = k$ , the total internal pressure is

$$\begin{aligned} \frac{P_e + P_b}{\rho g A} &= \frac{1}{4} (2 - e^{2ikL} - 2ikx) e^{ikx} - \frac{1}{4} e^{2ikL} e^{-ikx} \\ &= \frac{1}{2} [(1 - ikx) e^{ikx} - e^{2ikL} \cos kx]. \end{aligned} \quad (2.14)$$

From the second of equations (2.14), it can be seen that the travelling wave (which satisfies the bow boundary condition) has an initial amplitude equal to one-half of that of the external wave, and a component in quadrature with the external wave that grows linearly with  $x$ . When  $kx \gg 1$ , it leads the external wave by  $90^\circ$ .

It also follows from equation (2.14) that if  $L = n\pi/k$ , i.e. if the tube's length is an integer number of half wavelengths, the amplitude of the total internal pressure at the stern is  $n\pi/2$  times that of the external pressure.

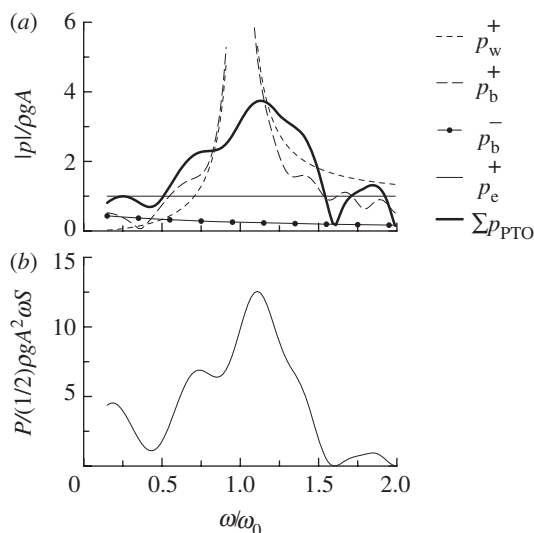


Figure 2. (a) Amplitudes of pressure in separate bulge wave components, as functions of normalized frequency. Superscripts + and – indicate the direction of travel. Subscripts denote the wave speed: w for the water wave, b for the free bulge wave. Thick line shows the pressure amplitude at the PTO. (b) Power converted in the PTO with an impedance that matches the tube. The length of the tube matches the water wavelength when  $\omega = \omega_0$ .

The mean power converted in the PTO,  $P = (1/2)S|P_e + P_b||U|$  at  $x = L$ , normalized with respect to the mean power that would be propagated in the undisturbed flow across the tube's frontal area, is

$$\frac{P}{(1/2)\rho g A^2 \omega S} = \frac{1}{8}[1 - \cos(2kL) + 2kL \sin(2kL) + 2k^2 L^2], \quad (2.15)$$

at resonance (assuming that the water waves are in deep water). Furthermore, if  $L = n\pi/k$ ,

$$\frac{P}{(1/2)\rho g A^2 \omega S} = \frac{n^2 \pi^2}{4}, \quad (2.16)$$

so that, if the tube is one wavelength long, the power gain is about 10. The capture width derived from equation (2.16) is  $n^2 \pi^2 k S/4$ .

It is interesting to note that the maximum power at the PTO occurs not when  $k_w = k_b$ , but at a slightly higher water wave frequency:  $k_w > k_b$ . In deep water conditions,  $k_w = \omega^2/g$  and  $k_b = \omega\omega_0/g$ , where  $\omega_0 = g/c$  is the frequency at which  $k_b = k_w$ . In figure 2a (in which the length of the tube is one wavelength at  $\omega/\omega_0 = 1$ ), the amplitudes of the four components of the internal pressure, namely  $p_w^+$ ,  $p_b^+$ ,  $p_b^-$  and the external pressure  $p_e^+$  are plotted as functions of the frequency ratio  $\omega/\omega_0$ . The first two of these approach very large values as  $\omega/\omega_0 \rightarrow 1$ , but they are in anti-phase. And since these functions are not symmetrical about  $\omega/\omega_0 = 1$ , the amplitude of the total normalized pressure at the PTO (shown as a heavy line, crossing  $\pi$  at  $\omega/\omega_0 = 1$ ), and the normalized power (figure 2b, crossing  $\pi^2$  at  $\omega/\omega_0 = 1$ ), reach maxima elsewhere, in this case at frequencies close

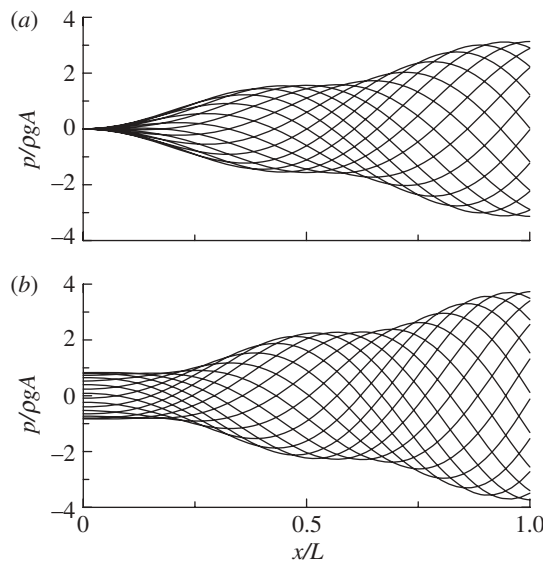


Figure 3. Theoretical pressures over the length of the tube at 16 instants over one period; (a)  $\omega/\omega_0 = 1$ ; (b)  $\omega/\omega_0 = 1.11$ , at which the PTO power is maximum.

to  $\omega/\omega_0 = 1.11$ . The computed progression of bulge waves is shown in figure 3, illustrating zero pressure at the bow for  $\omega/\omega_0 = 1$  (figure 3a), and higher PTO pressures for  $\omega/\omega_0 = 1.11$  (figure 3b).

(d) *Bulge wave propagation in the conditions of the experimental set-up*

Features of the experiments that can be included in a one-dimensional theoretical approach include finite hysteresis in the rubber wall of the tube, the presence of a slug of water between the end of the tube and the PTO, and non-matching PTO impedance. These issues are dealt with briefly here within the same theoretical framework, again neglecting the effect of wave diffraction and radiation.

As mentioned below in a description of the experiment, the oscillating flow at the end of the tube forced air back and forth through a large number of parallel capillary pipes, which provided a linear PTO of predictable and (by closing off some of the pipes) adjustable impedance. The layout is sketched in figure 4. The boundary conditions are  $U = 0$  at  $x = 0$  as before, and

$$\left\{ Z + iA' \frac{k_b}{K} \left[ 1 - \left( \frac{\omega}{\omega_0} \right)^2 W \right] \right\} U = \frac{P_b + P_e}{(\rho/D)^{1/2}} \quad \text{at } x = L, \quad (2.17)$$

where the impedance of the PTO is now  $Z\rho c/S$ , the length of the water slug is  $W/K$  with  $K = \omega_0^2/g$ , and  $A'$  is the ratio of the area of the tube to that of the water slug. If  $Z = 1$ , the PTO matches the tube impedance, and if  $W = 1$ , the natural frequency of the water slug is  $\omega_0$ .



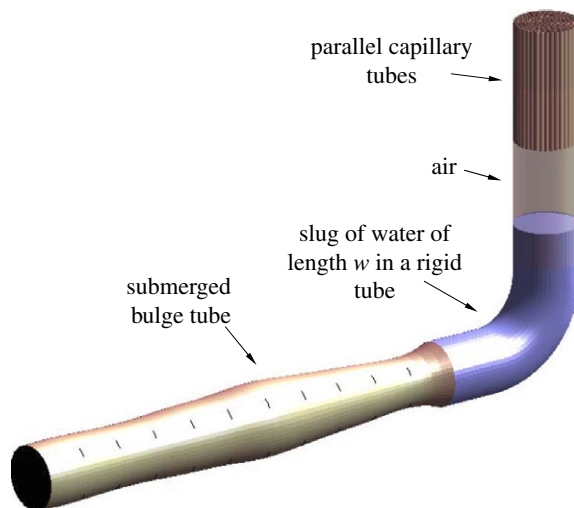


Figure 4. Elements of the experimental arrangement. (Online version in colour.)

The effect of hysteresis in the rubber is represented by an extra term on the right-hand side of the first of equations (2.6), which becomes

$$DS \frac{\partial}{\partial t} P_b(x) e^{-i\omega t} = \frac{\partial S}{\partial t} + \beta' \frac{\partial^2 S}{\partial t^2}, \quad (2.18)$$

where

$$\beta' = \left[ \frac{3}{4} \frac{r-1+\alpha}{\alpha - (r-1)^2} \right] \beta \quad (2.19)$$

and  $\tan^{-1} \beta \omega = \delta$  is the loss angle [1]. The fact that losses occur only in the rubber fraction of the circumference (which increases from its initial value  $\alpha$  as the tube expands), and that the rubber is assumed to be in a state of plane strain, accounts for the term in square brackets in equation (2.19). For small loss angles, the wave equation becomes

$$\frac{d^2 P_b}{dx^2} + \rho \omega^2 D (1 + i\beta' \omega) P_b = -\frac{d^2 P_w}{dx^2}. \quad (2.20)$$

The solution of equation (2.20) subject to the above boundary conditions reveals the three bulge wave components mentioned earlier. The bulge wave speed is reduced by the effect of hysteresis to become

$$\frac{\omega}{k_b} = \frac{1}{\sqrt{\rho D}} \frac{1}{\sqrt{\frac{1}{2}(1 + \sec \delta)}}. \quad (2.21)$$

The effects of mismatches between the impedances of the tube and the PTO, and between the resonant frequencies of the tube and the water slug, are shown in figure 5, where the normalized power is plotted as in figure 2*b* as a function of the frequency ratio. In this case, the effective loss angle  $\tan^{-1} \beta' \omega$  is  $10^\circ$ . In neither case is there a large change in the peak converted power.

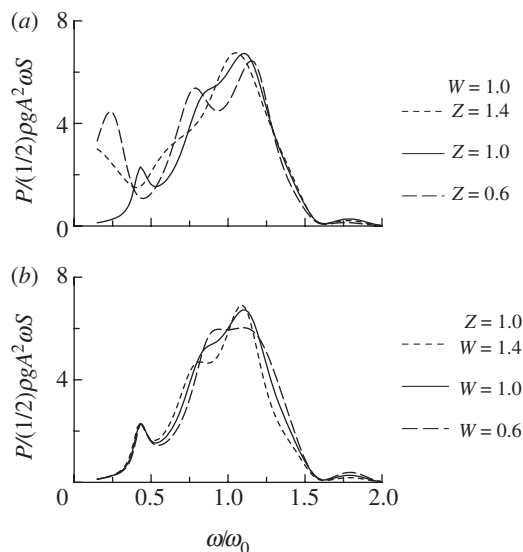


Figure 5. (a) Theoretical converted power for various PTO impedances  $Z$  and (b) for various slug lengths  $W$ . The effective loss angle is  $10^\circ$ . The length of the tube matches the water wavelength when  $\omega = \omega_0$ .

### 3. Experimental arrangements

#### (a) Basic set-up

These experiments were carried out in the towing tank at Southampton Solent University. The tank is 60 m long, 3.7 m wide, with a water depth of 1.87 m. The set-up is sketched in figure 6. The model Anaconda consisted of a 6.815 m long rubber tube of initial diameter 0.215 m, closed at the bow, and connected to a PTO system at the stern. In still water, the top of the tube was 40 mm below the water surface. The apparatus was mounted on the centreline of the tank, with the coordinate origin about 28 m from the wavemaker (a flap hinged at about mid-depth) and 27 m from the toe of the beach.

The tube was constructed from 1 mm thick rubber sheet. As mentioned earlier, four inelastic fabric strips were glued longitudinally to the external surface of the tube to delay the onset of aneurysm. Placed symmetrically, they covered 55 per cent of its circumference.

The requirements for the PTO were that it should behave like a linear dashpot, whose impedance could be adjusted over a range that bracketed that of the tube itself, while maintaining a positive internal pressure. Figure 6 shows a sketch of the actual system, which came very close to achieving these aims. At the stern, the rubber tube was connected to a stiff circular aluminium duct which turned upwards through a swept bend. The system was filled until the water surface inside the duct was 350 mm above the external free surface, providing the desired operating excess pressure in the rubber tube.

Above the internal water surface, the aluminium duct terminated with connections to 17 parallel 1 m long and 28 mm diameter copper pipes, open at their upper ends to the atmosphere. Each copper pipe was filled with about 140

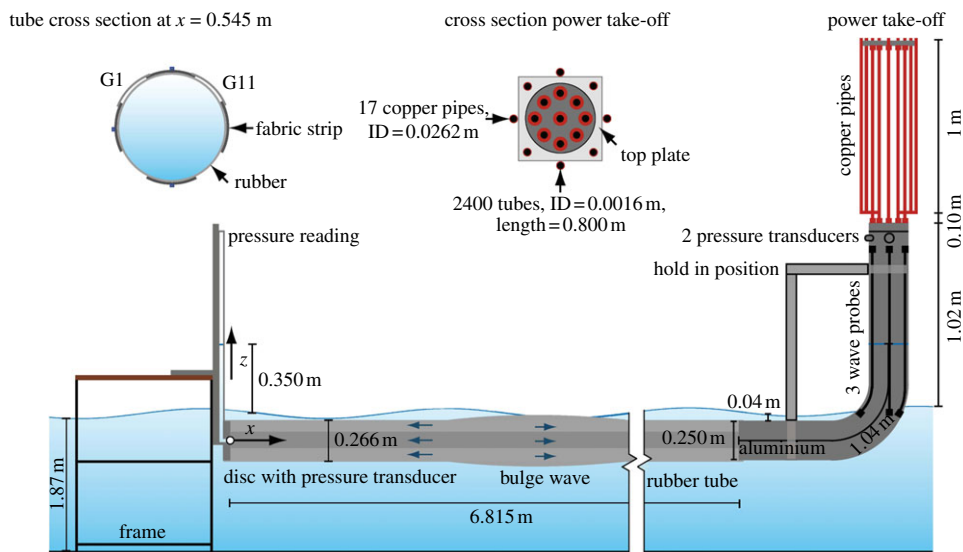


Figure 6. Experimental arrangement. (Online version in colour.)

parallel stainless steel pipes of internal diameter 1.6 mm and length 800 mm. The reversing flow in the rubber tube that accompanied the arrival of successive bulges at the PTO caused the slug of water inside the aluminium duct to oscillate, driving air backwards and forwards through the stainless steel pipes. The Reynolds number of this pipe flow, a few hundred, was well within the laminar regime. Other losses in the system were very much smaller, so the impedance of the PTO was essentially independent of both frequency and amplitude, and could be predicted with some confidence. It could be set between 37 and 481 kPa m<sup>-3</sup> s (0.64 <  $Z$  < 8.3) by closing off a number of copper pipes.

The length of the slug of water was 1.04 m. This is about 40 per cent less than that which would correspond to a natural frequency of  $\omega_0 = 2.60$  rads s<sup>-1</sup>, i.e.  $W \approx 0.6$ . However, according to the one-dimensional theory (figure 5), this is not likely to result in a large change in peak converted power.

Instrumentation included resistive wave gauges at several locations in the tank. The incident waves were monitored throughout the experiments, and checked later in the absence of all other apparatus. A pressure transducer was installed in the closed up-wave end of the tube. Other pressure transducers were fitted in the PTO between the internal water surface, whose elevation was recorded continuously with water surface elevation gauges, and the small-bore stainless steel pipes, as shown in figure 6. Data from these transducers provided both the impedance of the PTO and the power captured.

To measure circumferential strains in the rubber tube, we used gauges based on the liquid metal strain gauges originally developed by Whitney [20]. Those constructed for the present tests consisted of short silicone tubes with inner diameter 1 mm and wall thickness 0.5 mm, filled with Galinstan, a conducting alloy of gallium, indium and tin liquid at room temperature. The ends of the tubes were sealed with copper electrodes of 2 mm diameter, and the electrical

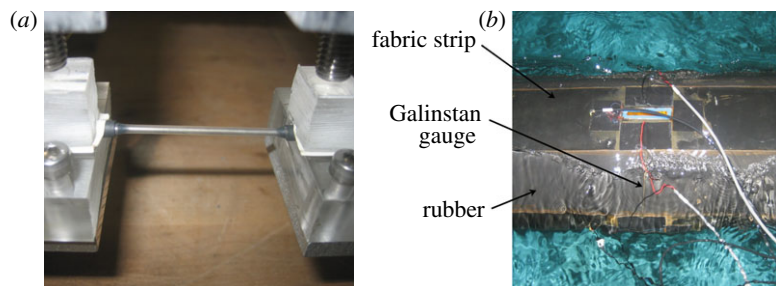


Figure 7. (a) Galinstan strain gauge under test. (b) Tube in the water. A Galinstan gauge can be seen bridging a section of rubber between two fabric strips. The wire gauge above it was not used in the present tests. (Online version in colour.)

resistance between them provided a measure of longitudinal strain. Attempts at manufacturing such gauges using a water–copper sulphate solution as electrolyte, like those described in an investigation of the motion of dracones [2,4], were not successful. We found that evaporation occurred, resulting in gas bubbles and loss of electrical continuity.

The 20 Galinstan gauges at 10 cross sections along the Anaconda tube had initial lengths of between 64 and 76 mm, and could be stretched by as much as 100 per cent. Their resistance was about  $0.6\ \Omega$  and their sensitivity about  $0.0004\ \Omega$  per per cent strain. Before installation, they were statically tested and found to be linear to within a few per cent, and dynamic tests showed their sensitivity to be independent of frequency over the range 0.4–4 Hz. On the model Anaconda they were aligned in the circumferential direction, spanning a section of rubber between adjacent fabric strips. The final calibration took place with the gauges fixed on the tube immediately before the tests, by varying the internal pressure and measuring the tube's circumference. Figure 7a shows a Galinstan gauge during testing on the bench, and figure 7b shows a gauge mounted on the tube in the tank.

### (b) *Tube calibrations*

Preliminary tests were carried out in still water to measure the distensibility of the tube and the speed of free bulge waves. Results of measurements of the tube's circumference at various internal pressures are shown in figure 8 in the form of tube areas as a function of pressure. They are seen to be in reasonable agreement with equation (2.1), based on Young's modulus of 1.3 MPa, which is consistent with the results of simple static extension tests on rubber samples. At the operating head of 350 mm (a pressure of 3.43 kPa—indicated by an arrow on the pressure axis in figure 8), the tube's area was  $0.055\ \text{m}^2$ .

An estimate of the free bulge wave speed in still water was obtained from tests in which a single bulge was generated by impulsive motion of a piston installed inside the tube at the bow. Data from the hoop strain gauges plotted in figure 9 record the passage of the bulge along the tube, at a mean speed of  $3.34\ \text{ms}^{-1}$ . In this case, the internal pressure was 3.17 kPa. The wavelength of the impulsively generated bulge was rather short (about 2 m) but even so the effect of longitudinal

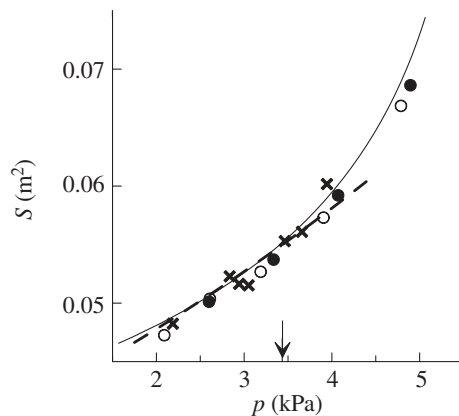


Figure 8. Cross-sectional areas of the tube inferred from static measurements of hoop strain at various internal pressures. Different symbols refer to measurements made on different occasions over the duration of the test programme. The solid line represents equation (2.1). The dashed line indicates the gradient  $dS/dp$  that corresponds to a bulge wave speed of  $3.20 \text{ m s}^{-1}$ . The operating internal pressure is indicated by an arrow on the pressure axis.

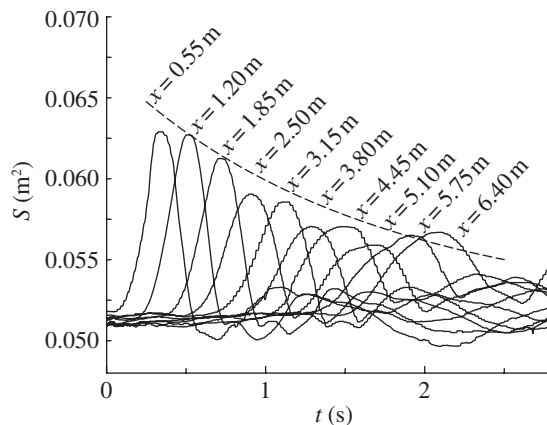


Figure 9. Tube cross-sectional areas inferred from hoop strain measurements, showing the progression of an impulsively generated bulge. The dashed line indicates the decay calculated for a loss angle of  $9^\circ$ .

curvature in raising the bulge wave speed (figure 1) would have been less than 1 per cent. Conversely, if the tube were deeply submerged, the surrounding water would slow the wave by about 5 per cent (equation (2.6)). As it is, the effect of the free surface is unknown.

According to equations (2.1) and (2.2), the effect of raising the internal pressure from 3.17 kPa (at which the measurement of wave speed was carried out) to the operating pressure of 3.43 kPa would be to reduce the wave speed from 3.34 to  $3.20 \text{ m s}^{-1}$ . The distensibility that corresponds to  $3.20 \text{ m s}^{-1}$  is seen (figure 8) to match the static measurements reasonably well, and this speed was

Table 1. PTO impedances and wave conditions.

series	$Z = \frac{\text{PTO impedance}}{\text{tube impedance}}$	wave periods (s)	number of wave amplitudes	number of tests
1	0.64	1.25–3.13	2	26
2	1.05	0.77–4.0	2	52
3	1.67	1.25–3.13	2	26
4	3.3	1.54–2.60	1	14
5	7.7	1.54–2.60	1	14
6	0.64–8.3	2.00	1	19
7	0.64–8.3	2.26	1	17

accordingly adopted for the purpose of identifying resonant water wave conditions in the experiments. The corresponding tube impedance is  $58.2 \text{ kPa m}^{-3} \text{ s}$ ; with a water depth of 1.87 m, the resonant water wave period was  $T_0 = 2.20 \text{ s}$  ( $\omega_0 = 2.86 \text{ rad s}^{-1}$ ).

The advancing bulge plotted in figure 9 lost energy to radiated waves and hysteresis in the tube wall. The latter would cause the internal pressure to decay as  $p \sim e^{-\gamma x}$ , with  $\gamma = \frac{1}{2} k \tan \delta$  [1]. On this basis, the dashed line in figure 9 indicates the progressive reduction in area that would be associated with a loss angle of  $\delta = 9^\circ$ . This is in reasonable agreement with the measurements. Dynamic tests on rubber taken from the tube wall indicated that the loss angle was about  $6^\circ$ , and it seems reasonable to assume that the additional losses in this test can be attributed to wave radiation.

#### 4. Experimental results and discussion

##### (a) Test conditions

The seven series of tests discussed below are identified in table 1. In each of the first five series, the impedance of the PTO was kept constant and measurements were made over a range of water wave periods  $T = 2\pi/\omega$  with wave amplitudes  $a$  in one or two ranges. In each of the last two series, the incident wave conditions were held constant, while the PTO impedance was varied over the whole available range.

Some typical time series are plotted in figure 10. Figure 10a shows the amplitudes of hoop strain increasing over the length of the tube between Galinstan gauges G2 and G10, while figure 10b confirms that the resistance of the PTO is in phase with the internal velocity. Since all signals were predominantly simple harmonic, higher frequency components were neglected in the analysis of the data.

##### (b) Bulge wave progression near resonance

On the assumption that cross sections of the tube remain circular, its areas  $S(x, t)$  at the 10 gauged sections over the length of the tube were computed from

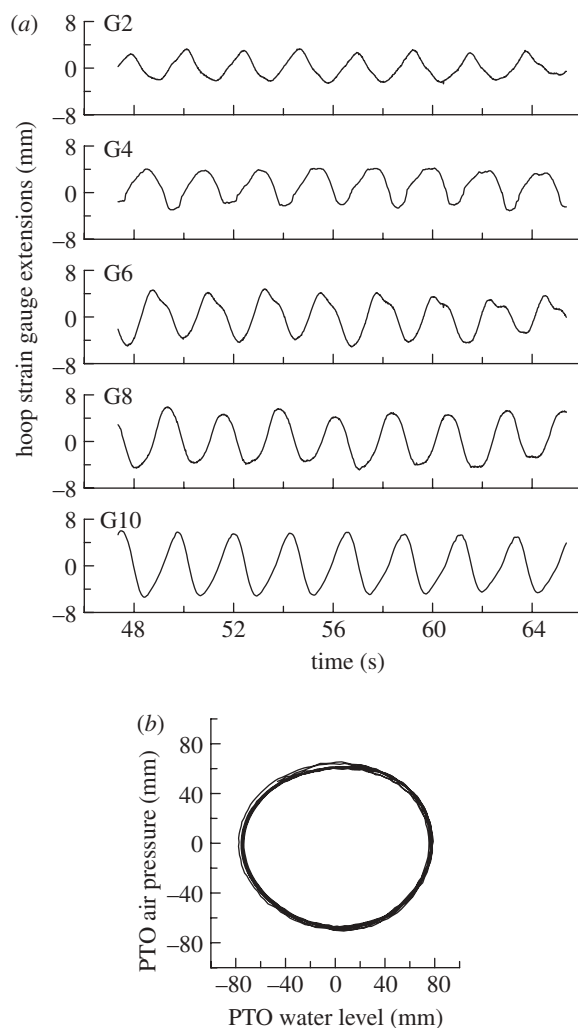


Figure 10. (a) Time series of extensions recorded by hoop strain gauges over the length of the tube from the bow (top) to the stern. (b) Water surface elevation in the PTO is in quadrature with air pressure. Series 2:  $T = 2.26$  s,  $a = 30$  mm.

the hoop strain signals. The total internal pressures  $p(x, t)$  then followed from a finite difference solution of the wave equation [1]

$$\frac{\partial^2 S}{\partial t^2} = \frac{S}{\rho} \frac{\partial^2 p}{\partial x^2}, \quad (4.1)$$

with boundary conditions provided by pressures measured at the bow and in the PTO. Estimates of the internal velocities  $u(x, t)$  could then be found by solving numerically the momentum equation  $\partial u / \partial t = -1/\rho (\partial p / \partial x)$ , with boundary conditions available from known velocities at each end. From these computed distributions of pressures and velocities, the mean forward propagation of power  $P(x)$  at points along the tube could be estimated.

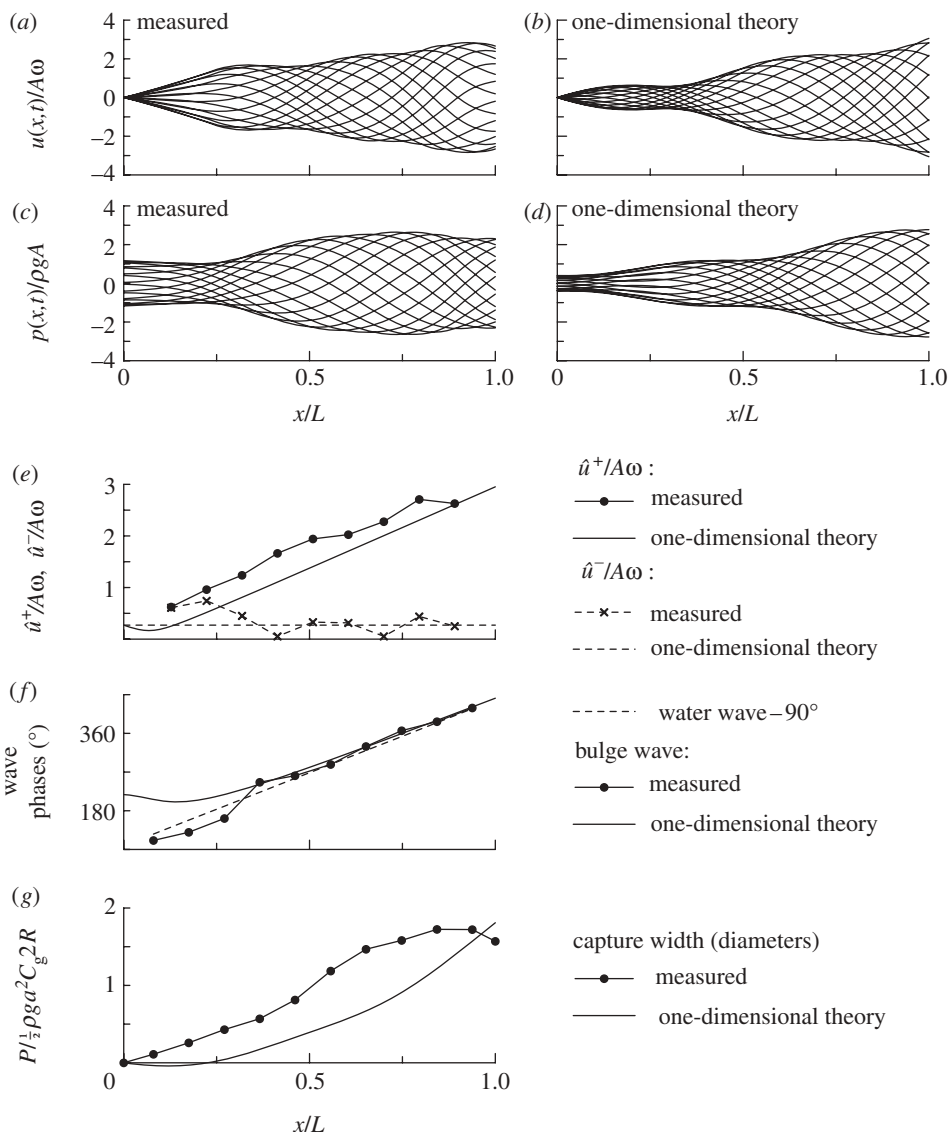


Figure 11. Internal particle velocities (a) inferred from measurements, and (b) calculated from one-dimensional theory, plotted over the length of the tube at 16 instants over one wave period; (c, d) corresponding total internal pressures; (e) forward- and backward-travelling bulge wave components, expressed in terms of corresponding particle velocity amplitudes  $\hat{u}^+$  and  $\hat{u}^-$ ; (f) measured and predicted phases of the forward-travelling bulge wave, plotted alongside the water wave phase shifted by  $90^\circ$ ; (g) power in the form of capture width in diameters ( $C_g$  is the group celerity). Series 2:  $T = 2.26$  s,  $a = 30$  mm,  $A = 29$  mm.

For the case shown in figure 10, very close to resonance, figure 11 compares several features of the measurements with predictions of the one-dimensional theory. Internal particle velocities and total internal pressures derived from the measurements at 16 instants over one wave period are plotted in figure 11a,c.



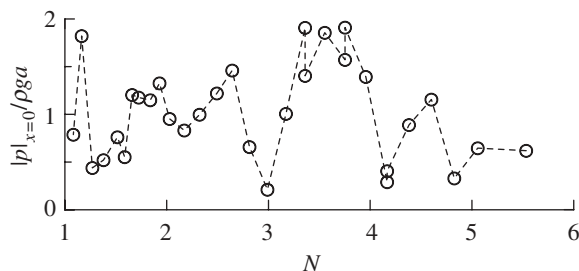


Figure 12. Amplitude of the internal bow pressure as a function of  $N = (k_w + k_b)L/2\pi$ . Series 3 tests,  $a = 30$  m.

They are normalized with respect to a representative wave particle velocity  $A\omega$  and a representative pressure  $\rho g A$ , where, in accordance with the definition adopted in §2,  $\rho g A$  is the amplitude of the pressure in the undisturbed waves at the elevation of the centre of the tube, in this case estimated from linear water wave theory. The lines in figure 11*a,c* are splines that pass through the measurements whose locations are identified by points in other plots in figure 11. Over the length of the tube, the maximum amplification of particle velocities and pressures both reach about 2.8. Figure 11*b,d* shows corresponding particle velocity and pressure distributions computed from the one-dimensional theory. Similar gains are seen, though the instantaneous profiles do not match very closely. Small differences in amplitudes and phases may be enough to have this effect.

In this case close to resonance, it is reasonable to assume that the bulges travel at the speed of the water waves, and then it becomes straightforward to separate the forward- and backward-travelling components of the internal waves by way of an algorithm set out in den Boer [21]. The amplitude of the internal velocity that is associated with each wave component is plotted in figure 11*e*. This shows that the forward-travelling bulge wave grows almost linearly with  $x$ , in accordance with the particle velocity implied by the corresponding part of the first of equations (2.14), shown as a solid line. Dashed lines represent the measured and predicted amplitudes of the reflected waves, which are much weaker and of almost uniform amplitude. In both cases, the measurements are in reasonable agreement with the one-dimensional theory.

Figure 11*f* shows the observed phase of the forward-travelling bulge waves. It is seen that their speed matches that of the water waves, and that they lead the water waves by about  $90^\circ$  in accordance with equation (2.14). The corresponding bulge wave phase obtained from equation (2.14) is shown as a solid line.

Measured and predicted power propagation is shown in the form of capture widths in figure 11*g*. The last measurement point represents the power actually converted in the PTO.

### (c) Bulge wave progression in other conditions

In other conditions (not necessarily at resonance), according to the discussion leading to equation (2.13), there should be cases in which the amplitude of the internal bow pressure falls to zero. This is tested in figure 12, where the measured

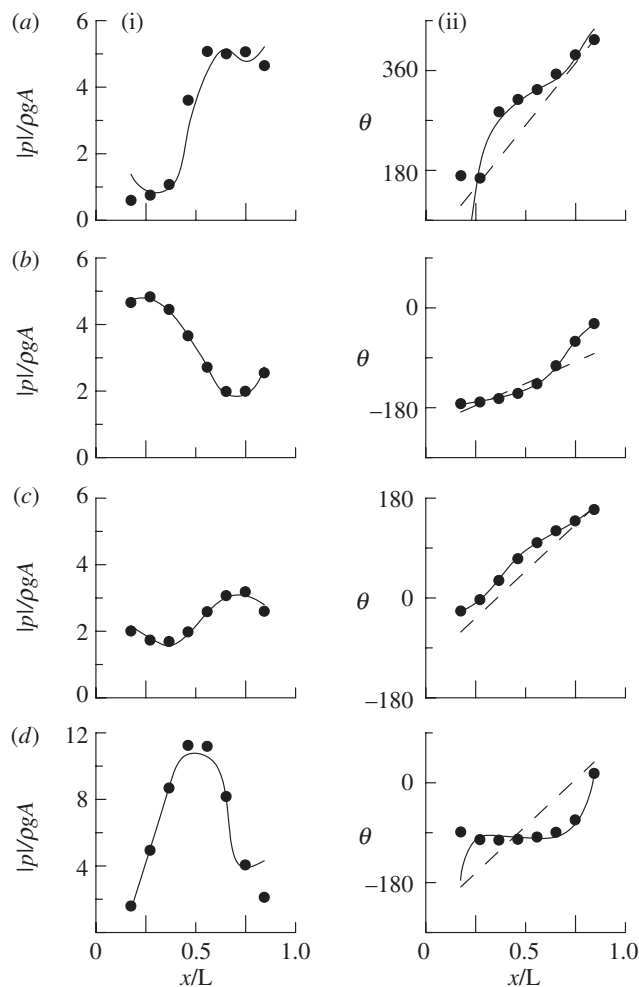


Figure 13. (i) Measured amplitudes of total internal pressure and (ii) phases over the length of the tube, plotted as points. Solid lines represent the sum of three bulge wave components with amplitudes computed by least squares. Dashed lines represent the measured phase of the water waves with a shift of  $90^\circ$ . (a) Series 2:  $T = 1.90$  s,  $a = 26$  mm; (b) series 2:  $T = 4.0$  s,  $a = 46$  mm; (c) series 7:  $Z = 0.64$ ,  $a = 30$  mm; (d) series 7:  $Z = 3.4$ ,  $a = 30$  mm.

pressure is plotted against  $N = (k_w + k_b)L/2\pi$ . Some confirmation of the theory is provided by the fact that the pressure amplitudes are highly modulated and exhibit minima close to integer values of  $N$ .

In general, most of the motion inside the tube can be explained as the sum of the three components of uniform amplitudes identified in the one-dimensional theory; namely, bulge waves travelling forwards with speeds  $\omega/k_w$  and  $\omega/k_b$ , and another going in the opposite direction at  $\omega/k_b$  (equation (2.10)). Their respective pressure amplitudes  $|P_w^+|$ ,  $|P_b^+|$  and  $|P_b^-|$  were estimated from the inferred pressures in the tube by a least-squares method. Data in figure 13 support this approach, showing that, over a wide range of conditions, amplitudes  $|P|$  and

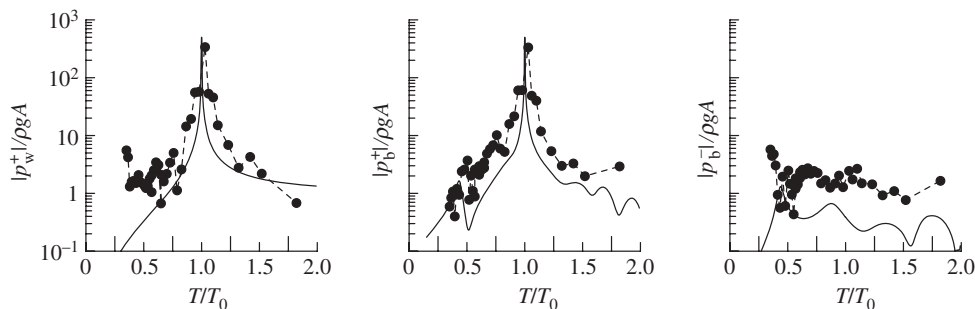


Figure 14. Amplitudes of the three constituent bulge waves in series 2 tests plotted as functions of relative wave period. Symbols represent the amplitudes obtained from pressures inferred from measurements; lines show the amplitudes of the same component waves obtained from equation (2.10) for the experimental conditions.

phases  $\theta$  of measured pressures at all points within the tube are in reasonable agreement with those obtained by combining the three pressure waves.

A more severe test is to compare the pressure amplitudes of the three constituent waves with those computed directly from the one-dimensional theory for the same conditions. These results are plotted in figure 14 for all tests in series 2. The pressures are normalized with respect to  $\rho g A$ , which in the case of the measurements is the estimated pressure amplitude at the elevation of the centre of the tube in the undisturbed waves. There are strong similarities, though quantitative agreement between experimental and predicted data is not very good, and, as in figure 11, the pressures based on measurements are generally higher than the predictions.

#### (d) Power capture

Setting the impedance of the PTO higher than that of the tube results in high pressures in the PTO, and low amplitudes of motion. If the impedance is low, the reverse is true. At a given wave frequency, the condition for maximum converted power is likely to be when the impedance of the PTO matches that of the tube. In this condition, if the device had a simple dashpot PTO, were in deep water and tuned to the wave frequency, the free bulge wave speed would be  $c_b = g/\omega$  and the impedance  $\rho c_b/S = \rho g/\omega S$ . Then the relationship between pressure  $p_{PTO}$  and velocity  $u_{PTO}$  in the PTO would be  $p_{PTO} = (\rho g/\omega S)u_{PTO}S$ , and the amplitude of the motion in the PTO would be the same as the amplitude of the pressure head:  $a_{PTO} = u_{PTO}/\omega = p_{PTO}/\rho g$ .

This exchange between PTO pressure and displacement is illustrated in figure 15 over a range of impedances at two wave frequencies. The points show measurements, and the lines are computed from the one-dimensional theory outlined in §2d. As expected, the intersection occurs close to  $Z=1$ . The measurements are in close agreement with the theoretical data calculated for a loss angle of  $9^\circ$ , which also provided a good prediction for the decay of free bulge waves in still water (figure 9), probably representing losses owing to both hysteresis and wave radiation.

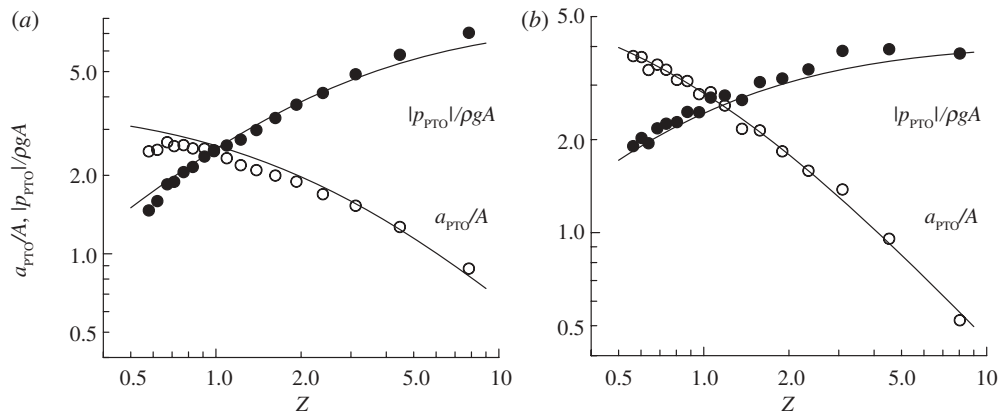


Figure 15. Points show measured (filled circles and open circles) pressures and amplitudes of motion in the PTO from tests in (a) series 6 ( $T/T_0 = 0.91$ ) and (b) series 7 ( $T/T_0 = 1.03$ ) as functions of PTO impedance. At  $Z = 1$ , the PTO impedance matches the tube impedance. Lines represent results computed from the one-dimensional theory, §2d:  $\delta = 9^\circ$ .

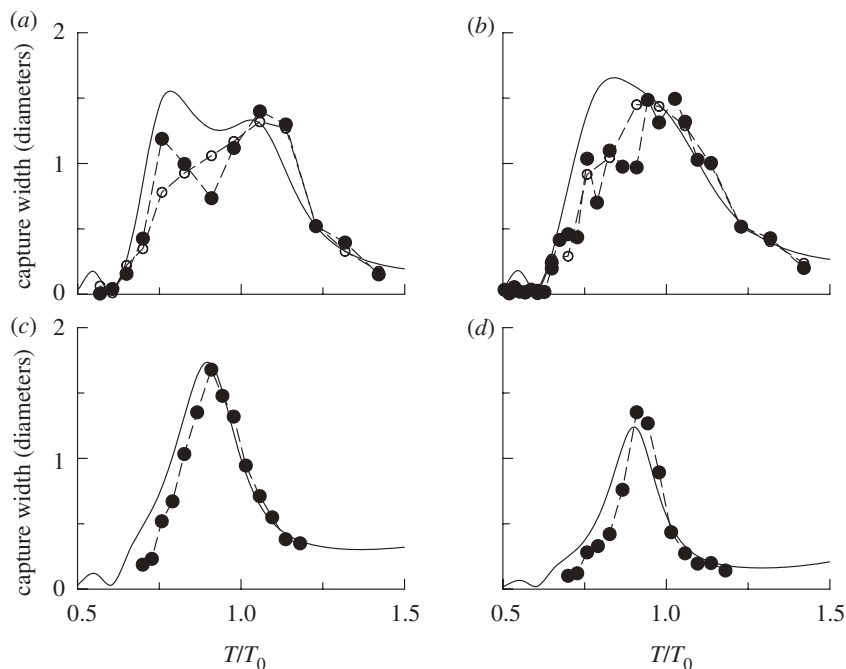


Figure 16. Capture widths as functions of relative wave period for (a)  $Z = 0.64$ , (b)  $Z = 1.05$ , (c)  $Z = 3.3$ , (d)  $Z = 7.7$ . Measurements are shown as points; one-dimensional theory with  $\delta = 9^\circ$  as solid lines.

Capture widths for four different PTO impedances are plotted in figure 16 as functions of relative wave period. The measurements are in reasonable agreement with the theoretical results, computed with  $\delta = 9^\circ$ . The peak power seems not to be much affected by the PTO impedance for  $Z < 3.3$ , but the power curve

becomes narrower as the impedance is increased. At the higher impedances, the power peaks at wave periods below that corresponding to resonance as expected, but there is not much evidence of this at the lowest impedances.

## 5. Conclusions

Experiments have been carried out on a model of the Anaconda wave energy converter at a scale of about 1:25 in regular waves. The device consists of a distensible tube in which wave energy is captured in the form of internal oscillating flow. The model was equipped with a linear PTO of adjustable impedance. Measurements of the distensibility of the tube and of the speed of free bulge waves in the tube in still water agreed closely with predictions based on known material properties.

During tests in waves, liquid metal strain gauges provided recordings of hoop strain at 10 sections along the length of the tube, from which internal velocities, pressures and the propagation of power were estimated. Peak capture widths were less than two diameters, but the test conditions were not necessarily optimized to achieve maximum power conversion.

Many features of the measurements were in surprisingly good agreement with the predictions of a one-dimensional model for the Anaconda, based on the assumptions that the tube remains straight and horizontal, and that the effects of water wave diffraction and radiation can be neglected. However, development of the theory did involve some issues that do not arise in the analysis of wave propagation in distensible tubes in other contexts, e.g. the effects of inelastic sectors of the circumference, longitudinal tension and the presence of the surrounding water.

According to the theory, the fluid motion in the tube can be interpreted as the sum of three distinct bulge wave components, one travelling forwards at the water wave speed and one travelling in each direction at the free bulge wave speed. The backward-travelling wave is much smaller than the others. At resonance (when the speeds of the water waves and free bulge waves match), the forward-travelling bulge waves grow linearly with distance along the tube, leading the water waves by  $90^\circ$ . These conclusions were strongly supported by measurements over a wide range of frequencies and PTO impedances. Quantitative agreement between many measured and predicted parameters, including capture widths, was improved by adopting a slightly higher level of hysteresis in the theory than that which could be attributed to energy losses in the tube wall. It seems likely that this would be unnecessary in a theory which included the effects of wave diffraction and radiation.

This work was supported by the EPSRC (grant no. EP/F030975/1). The authors also thank Checkmate SeaEnergy for the provision of rubber tubes, and for helpful discussions.

## References

- 1 Farley, F. J. M., Rainey, R. C. T. & Chaplin, J. R. 2012 Rubber tubes in the sea. *Phil. Trans. R. Soc. A* **370**, 381–402. (doi:10.1098/rsta.2011.0193)
- 2 Hawthorne, W. R. 1961 The early development of the dracone flexible barge. *Proc. Inst. Mech. Eng.* **175**, 52–83. (doi:10.1243/PIME\_PROC\_1961\_175\_011\_02)

- 3 Zhao, R. & Triantafyllou, M. 1994 Hydroelastic analyses of a long flexible tube in waves. In *Hydroelasticity in marine technology* (eds O. Faltinsen, C. M. Larsen & T. Moan), pp. 287–300. Trondheim, Norway: Balkema.
- 4 Fish, D. C. E. 1965 Strain measurement on the dracone flexible barge. *Strain* **1**, 14–20. (doi:10.1111/j.1475-1305.1965.tb00048.x)
- 5 van de Vosse, F. N. & Stergiopoulos, N. 2011 Pulse wave propagation in the arterial tree. *Annu. Rev. Fluid Mech.* **43**, 467–499. (doi:10.1146/annurev-fluid-122109-160730)
- 6 Graff, K. F. 1975 *Wave motion in elastic solids*. Oxford, UK: Clarendon Press.
- 7 Pedley, T. J. 1980 *The fluid mechanics of large blood vessels*. Cambridge, MA: Cambridge University Press.
- 8 Gerrard, J. H. 1985 An experimental test of the theory of waves in fluid-filled deformable tubes. *J. Fluid Mech.* **156**, 321–347. (doi:10.1017/S0022112085002129)
- 9 Horsten, J. B. A. M., Vansteenhoven, A. A. & Vandongen, M. E. H. 1989 Linear propagation of pulsatile waves in viscoelastic tubes. *J. Biomech.* **22**, 477–484. (doi:10.1016/0021-9290(89)90208-X)
- 10 Li, J. K., Melbin, J., Riffle, R. A. & Noordergraaf, A. 1981 Pulse-wave propagation. *Circ. Res.* **49**, 442–452. (doi:10.1161/01.RES.49.2.442)
- 11 Womersley, J. R. 1957 Oscillatory flow in arteries: the constrained elastic tube as a model of arterial flow and pulse transmission. *Phys. Med. Biol.* **2**, 178–187. (doi:10.1088/0031-9155/2/2/305)
- 12 Moodie, T. B. & Barclay, D. W. 1986 Wave propagation and reflection in liquid filled distensible tube systems exhibiting dissipation and dispersion. *Acta Mech.* **59**, 139–155. (doi:10.1007/BF01181661)
- 13 Moodie, T. B., Barclay, D. W. & Greenwald, S. E. 1986 Impulse propagation in liquid filled distensible tubes: theory and experiment for intermediate to long wavelengths. *Acta Mech.* **59**, 47–58. (doi:10.1007/BF01177059)
- 14 Moodie, T. B., Barclay, D. W., Greenwald, S. E. & Newman, D. L. 1984 Waves in fluid filled tubes: theory and experiment. *Acta Mech.* **54**, 107–119. (doi:10.1007/BF01190600)
- 15 Young, T. 1808 Hydraulic investigations, subservient to an intended Croonian lecture on the motion of the blood. *Phil. Trans. R. Soc. Lond.* **98**, 164–186. (doi:10.1098/rstl.1808.0014)
- 16 Lighthill, J. 1978 *Waves in fluids*. Cambridge, MA: Cambridge University Press.
- 17 Newman, D. L., Greewald, S. E. & Moodie, T. B. 1983 Reflection from elastic discontinuities. *Med. Biol. Eng. Comput.* **21**, 697–701. (doi:10.1007/BF02464032)
- 18 Ursino, M., Artioli, E. & Gallerani, M. 1993 Wave-propagation with different pressure signals: an experimental-study on the latex tube. *Med. Biol. Eng. Comput.* **31**, 363–371. (doi:10.1007/BF02446689)
- 19 Turner, D. M. & Brennan, M. 1990 The multiaxial elastic behaviour of rubber. *Plast. Rubber Process. Appl.* **14**, 183–188.
- 20 Whitney, R. J. 1953 The measurement of volume changes in human limbs. *J. Physiol.* **121**, 1–27.
- 21 den Boer, K. 1981 Estimation of incident and reflected wave characteristics of perpendicular wave action. Research report S4341981. Delft Hydraulics Laboratory, Delft, The Netherlands.